12380–12393 *Nucleic Acids Research, 2020, Vol. 48, No. 21* *Published online 10 November 2020*
doi: 10.1093/nar/gkaa1001

On the interaction of an anticancer trisubstituted naphthalene diimide with G-quadruplexes of different topologies: a structural insight

Chiara Platella[1], Marko Trajkovski[2], Filippo Doria[3], Mauro Freccero[3], Janez Plavec[2,4,5,*] and Daniela Montesarchio[1,*]

[1]Department of Chemical Sciences, University of Naples Federico II, via Cintia 21, I-80126 Naples, Italy, [2]Slovenian NMR Centre, National Institute of Chemistry, Hajdrihova 19, SI-1000 Ljubljana, Slovenia, [3]Department of Chemistry, University of Pavia, Viale Taramelli 10, I-27100 Pavia, Italy, [4]EN→FIST Centre of Excellence, Trg OF 13, SI-1000 Ljubljana, Slovenia and [5]Faculty of Chemistry and Chemical Technology, University of Ljubljana, Večna pot 113, SI-1000 Ljubljana, Slovenia

Received July 06, 2020; Revised September 29, 2020; Editorial Decision October 13, 2020; Accepted October 22, 2020

ABSTRACT

Naphthalene diimides showed significant anticancer activity in animal models, with therapeutic potential related to their ability to strongly interact with G-quadruplexes. Recently, a trifunctionalized naphthalene diimide, named NDI-5, was identified as the best analogue of a mini-library of novel naphthalene diimides for its high G-quadruplex binding affinity along with marked, selective anticancer activity, emerging as promising candidate drug for in vivo studies. Here we used NMR, dynamic light scattering, circular dichroism and fluorescence analyses to investigate the interactions of NDI-5 with G-quadruplexes featuring either parallel or hybrid topology. Interplay of different binding modes of NDI-5 to G-quadruplexes was observed for both parallel and hybrid topologies, with end-stacking always operative as the predominant binding event. While NDI-5 primarily targets the 5′-end quartet of the hybrid G-quadruplex model (m-tel24), the binding to a parallel G-quadruplex model (M2) occurs seemingly simultaneously at the 5′- and 3′-end quartets. With parallel G-quadruplex M2, NDI-5 formed stable complexes with 1:3 DNA:ligand binding stoichiometry. Conversely, when interacting with hybrid G-quadruplex m-tel24, NDI-5 showed multiple binding poses on a single G-quadruplex unit and/or formed different complexes comprising two or more G-quadruplex units. NDI-5 produced stabilizing effects on both G-quadruplexes, forming complexes with dissociation constants in the nM range.

GRAPHICAL ABSTRACT

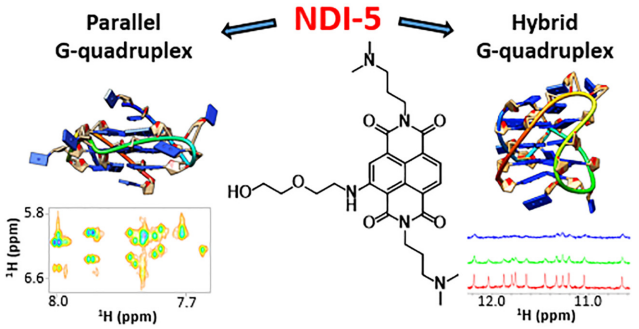

INTRODUCTION

Cancer is the second leading cause of death worldwide (1). Considering invasiveness of tumour cells and the fact that each tumour form requires *ad hoc* therapeutic regimen, fighting cancer is not trivial (2). In the last decades, scientific research moved forward in cancer treatment by developing targeted therapies, featured by low-to-null toxicity, as valid and effective alternatives to conventional chemotherapies (3–6). Several antitumor targets were discovered and, among them, a strong interest arose for non-canonical nucleic acid structures known as G-quadruplexes, found at oncogene promoters and telomeres (7–13). G-quadruplexes are secondary structures of DNA and/or RNA formed by stacking of cyclic planar arrangements of four guanines called G-quartets, and stabilized by metal cations (7–13). These peculiar nucleic acid architectures play key roles in the regulation of tumour-specific genes as well as in molecular pathways involved in uncontrolled proliferation mechanisms typical of all tumour types. Thus, selectively target-

*To whom correspondence should be addressed. Tel: +39 081 674126; Fax: +39 081 674313; Email: daniela.montesarchio@unina.it
Correspondence may also be addressed to Janez Plavec. Tel: +386 1 47 60 353; Fax: +386 1 47 60 300; Email: janez.plavec@ki.si

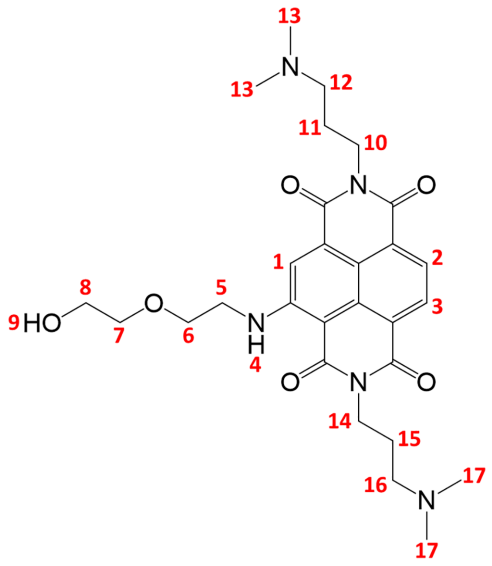

Figure 1. Chemical structure of naphthalene diimide **NDI-5** with atom numbering used in this study.

ing G-quadruplex structures *in vivo* represents a very general and promising anticancer strategy (7–12,14,15).

The appealing possibility to treat common features of different cancers without impairing normal cells stimulated the synthesis of large libraries of putative selective G-quadruplex ligands. To rapidly and effectively select 'true hits', an affinity chromatography-based method, i.e. the G4-CPG (G-quadruplex on Controlled Pore Glass) assay, has been recently developed to identify ligands able to specifically recognize biologically relevant G-quadruplex structures (16–20). More specifically, we recently focused on a library of new multifunctionalized naphthalene diimides (NDIs) (21). NDIs have a remarkable potential as anticancer drugs because of their well-proven ability to interact with G-quartets (22–26). Moreover, their effective antitumor activity was demonstrated in several *in vivo* studies (27–33). By exploiting the G4-CPG assay, **NDI-5** (Figure 1) was found to be the most attractive compound within the investigated series, and thus further analyzed by circular dichroism (CD) and fluorescence experiments (21). Noteworthy, biological assays underpinned **NDI-5** as a promising candidate drug due to its strong and selective activity against cancer cells, showing IC_{50} value of 79 nM on HeLa cells (21).

Encouraged by these results, we deemed it essential to undertake an in-depth study on the interaction of **NDI-5** with G-quadruplexes to clarify the structural details of this strong and specific binding. Here, we reported a detailed NMR investigation on the **NDI-5** interactions with G-quadruplexes of different structural topologies, complemented with dynamic light scattering (DLS), CD and fluorescence spectroscopy analyses. The DNA models of choice comprised G-rich oligonucleotides able to fold into stable and well-characterized G-quadruplex structures, i.e. M2 and m-tel24, respectively exhibiting parallel and hybrid-1 type topologies (Figure 2A and B) (34,35).

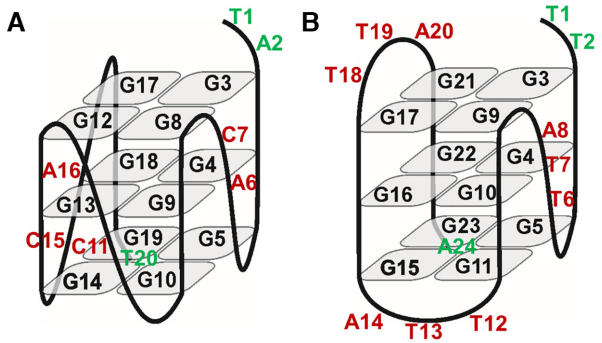

Figure 2. Schematic representation of G-quadruplex structures adopted by: (**A**) M2 (34) and (**B**) m-tel24 (35). Guanines forming the G-quartets, loop residues and 5′- and 3′-end flanking residues are represented with black, red and green labels, respectively.

The primary sequences of the herein used model oligonucleotides, M2 *d*(TAGGGACGGGCGGGCAGGGT) and m-tel24 *d*[TTGGG(TTAGGG)$_3$A], are in line with vastly accepted consensus motif for G-quadruplex formation. M2 G-quadruplex exhibits all strands in parallel orientation, a common feature of most G-quadruplex-forming DNA segments in oncogene promoter regions (34). On the other hand, m-tel24 comprises the sequence originating from human telomeric DNA which has been only slightly modified to favour hybrid-1 G-quadruplex topology (35) and reduce the high polymorphism of telomeric DNA, thus allowing a detailed NMR investigation (36,37). Structural characterization of G-quadruplex/**NDI-5** complexes was aimed at elucidating the binding of **NDI-5** to both parallel and hybrid topologies, so to better guide the future rational design of optimized **NDI-5** analogues in the quest for effective anticancer drugs.

MATERIALS AND METHODS

Sample preparation

Non-labelled, modified and residue-specific low-enrichment (10%) ^{15}N- and ^{13}C-labelled DNA oligonucleotides were synthesized on H-8 synthesizer (K&A LaborGeräte) with the use of standard phosphoramidite chemistry and then deprotected with aqueous ammonia. Purification and desalting of DNA oligonucleotides were performed by means of Amicon-15 centrifuge filter with 3.0 kDa MWCO. The oligonucleotide concentration was determined by measuring the absorbance at 260 nm and 90°C, using the appropriate molar extinction coefficients (38). **NDI-5** was synthesized and purified as previously described (21). The **NDI-5** stock solution was prepared by dissolving the solid compound in aqueous solution at 100 mM KCl, 20 mM potassium phosphate buffer (pH 7), 90%/10% H_2O/D_2O, at 20 mM concentration of the ligand for NMR studies or in pure water at 4 mM concentration of the ligand for DLS, CD and fluorescence analyses.

NMR experiments

NMR data were collected on Agilent NMR Systems 600 and 800 MHz and on Bruker AVANCE NEO 600 MHz

NMR spectrometers in the range 0–50°C. Oligonucleotide samples were prepared in 100 mM aqueous KCl, 20 mM potassium phosphate buffer (pH 7), 90%/10% H_2O/D_2O, at 0.2 mM oligonucleotide concentration per strand. In titration experiments, aliquots of the **NDI-5** stock solution were directly added to the oligonucleotide solutions inside the NMR tube. NMR spectra were acquired with the use of the DPFGSE solvent suppression method. Unambiguous assignment of imino, aromatic and methyl ^{1}H NMR resonances was done with the aid of ^{15}N- and ^{13}C-HSQC spectra. Between sixty and twenty different gradient strengths (1–60 G·cm^{-1}) were used in DOSY NMR experiments. From translation diffusion coefficients (D_t) obtained from DOSY experiments, hydrodynamic dimensions for M2 and m-tel24 in the absence and presence of **NDI-5** was calculated by using Stokes–Einstein equation (39):

$$D_t = k_B T/3\pi\eta D_h \rightarrow D_h = k_B T/3\pi\eta D_t$$

where D_h is the hydrodynamic diameter, k_B is the Boltzmann constant (1.38×10^{-23} m^2·kg·K·s^{-2}), T is the temperature (298.15 K), η is the fluid viscosity for 90%/10% H_2O/D_2O solution, calculated as previously described (0.917 mPa·s) (40) and D_t is the experimentally determined diffusion coefficient. NOESY spectra were acquired at mixing times between 80 and 500 ms. TOCSY spectrum was acquired at mixing time of 60 ms. ROESY spectra for **NDI-5** and for M2 in presence of **NDI-5** were acquired at mixing time in the range from 60 to 300 ms. For the NMR-monitored experiments evaluating the ability of **NDI-5** to induce M2 G-quadruplex structuring in metal cation-free buffers, a 0.2 mM solution of M2 oligonucleotide was prepared in 90%/10% H_2O/D_2O and 6 molar equivalents of **NDI-5** added to the oligonucleotide solution. DSS (4,4-dimethyl-4-silapentane-1-sulfonic acid) was used as a reference to calibrate the chemical shifts, assuming that DSS resonates at 0.0 ppm. NMR spectra were processed and analyzed with the use of VNMRJ (Varian Inc.), TopSpin 4.0.7 (Bruker) and Sparky (UCSF) softwares.

DLS experiments

DLS measurements were performed on a Zetasizer Nano ZS. M2 and m-tel24 samples were prepared at 1 mg/mL concentration respectively corresponding to 0.16 and 0.13 mM in 100 mM aqueous KCl and 20 mM potassium phosphate buffer (pH 7) and titrated with increasing amounts of **NDI-5** (from 1 to 6 molar equivalents). The experiments were carried out at 25°C at a scattering angle θ of 175° (backscatter detection). The diffusion coefficient of each population was calculated from the correlation function. The Stokes-Einstein equation was then used to evaluate the hydrodynamic diameter of free M2 and m-tel24, as well as of their complexes with **NDI-5**, from the related diffusion coefficients (39). Errors on hydrodynamic diameter were calculated as standard deviation of three independent measurements.

CD experiments

CD spectra were recorded in quartz cuvettes with a path length of 1 or 0.1 cm on a Jasco J-715 spectropolarimeter equipped with a Peltier-type temperature control system (model PTC-348WI). The spectra were recorded at 20°C in the range 240–800 nm with 2 s response, 200 nm/min scanning speed, 2.0 nm bandwidth, and corrected by subtraction of the background scan with buffer. All the spectra were averaged over 3 scans. Oligonucleotide samples were dissolved in a 20 mM aqueous KCl and 5 mM potassium phosphate buffer (pH 7) to obtain 2 μM solutions, then annealed by heating at 95°C for 5 min, followed by slow cooling to room temperature. CD titrations were obtained by adding increasing amounts of the ligands to M2 or m-tel24 G-quadruplexes. The ligand was added to each oligonucleotide solution until saturation of the oligonucleotide CD signals was achieved, which corresponded to 6 molar equivalents. After each ligand addition, the system was allowed equilibrating before recording the spectra. For the CD-melting experiments, the ellipticity was recorded at 265 or 290 nm, respectively for M2 and m-tel24, with a temperature scan rate of 0.5°C/min in the range 20–90°C. For the CD-monitored experiments evaluating the ability of **NDI-5** to induce G-quadruplex structuring in metal cation-free buffers, 20 μM solutions of M2 or m-tel24 oligonucleotides were prepared in 10 mM Tris–HCl buffer (pH 7) and m-tel24 was titrated with increasing amounts of **NDI-5** (up to 6 molar equivalents). The melting curve for the 1:6 m-tel24:**NDI-5** ratio mixture was recorded at 290 nm, with a temperature scan rate of 0.5°C/min, in the range 10–90°C.

Fluorescence experiments

Fluorescence spectra were recorded at 20°C on HORIBA Jobin Yvon Inc. FluoroMax®-4 spectrofluorometer equipped with F-3004 Sample Heater/Cooler Peltier Thermocouple Drive, by using a quartz cuvette with a 1 cm path length. **NDI-5** was excited at 526 nm and emission spectra were recorded between 540 and 800 nm. Both excitation and emission slits were set at 5 nm. The experiments were performed in 20 mM aqueous KCl and 5 mM potassium phosphate buffer (pH 7). For fluorescence titration experiments, 2 μM ligands solutions were prepared in 20 mM KCl and 5 mM potassium phosphate buffer (pH 7). Increasing amounts of M2 or m-tel24 (up to 4 μM concentration) were added from 120 μM stock solutions of each DNA sample annealed in 20 mM KCl and 5 mM potassium phosphate buffer (pH 7). After each addition, the system was allowed equilibrating 10–15 min before recording the spectra. The fraction of bound ligand was calculated from the fluorescence intensity at 589 nm and reported in graph as a function of the DNA concentration. The obtained points were fitted with an independent and equivalent-sites model (41) using the Origin 8.0 program with the following equation:

$$\alpha = \left(\frac{1}{2[L]_0}\right)\left\{\left([L]_0 + n[Qu] + \frac{1}{K_b}\right) - \sqrt{\left([L]_0 + n[Qu] + \frac{1}{K_b}\right)^2 - 4[L]_0 n[Qu]}\right\}$$

where α is the molar fraction of ligand in the bound form, $[L]_0$ is the total ligand concentration, $[Qu]$ is the added oligonucleotide concentration, n is the number of the equivalent and independent sites on the target DNA structure

and K_b is the binding constant. The fraction of the bound ligand was determined using the equation:

$$\alpha = \frac{Y - Y_0}{Y_b - Y_0}$$

where Y, Y_0 and Y_b are the values of fluorescence emission intensity at the maximum, respectively, at each titrant concentration, at the initial state and the final state of the titration. The errors associated to the binding constant values are based on the fit and n was considered fixed at 3 and 4 for M2 and m-tel24 systems, respectively.

For the construction of the Job plot, the molar fraction of **NDI-5** was varied from 0 to 1 and the total molar concentration ([ligand] + [DNA]) was kept constant at 2 μM. Job plot experiments were performed in duplicate and the error associated with the molar fraction values of **NDI-5** in correspondence of the slope changes was found to be within ±0.01.

RESULTS AND DISCUSSION

NMR studies

*NMR analysis of the G-quadruplex models and naphthalene diimide **NDI-5**.* The interaction of **NDI-5** with parallel M2 and hybrid-1 m-tel24 G-quadruplexes was studied at 100 mM KCl and 20 mM potassium phosphate buffer (pH 7.0). Under these conditions, both models gave high quality NMR spectra, with the predominant G-quadruplex conformation accounting in solution for >95% of the whole nucleotide material. Twelve narrow and well-resolved imino proton signals were observed in the ^{1}H NMR spectrum of M2, consistent with the formation of a G-quadruplex with three G-quartets (Figure 3, bottom). In detail, M2 adopts a parallel G-quadruplex consisting of three stacked G-quartets, i.e. G3:G8:G12:G17, G4:G9:G13:G18 and G5:G10:G14:G19, sandwiched between the 5′- and 3′-end flanking residues (T1-A2 and T20, respectively) and connected by three propeller-type loops involving A6-C7, C11 and C15-A16 residues (Figure 2A). Notably, the M2 G-quadruplex studied herein showed identical structural features as the one analyzed in a previous study, adopting the same experimental conditions (34).

In comparison, our NMR analysis on m-tel24 was carried out at slightly higher K^+ concentration than in previously published studies (100 mM KCl versus 70 mM KCl) (35). Hence, we used 2D-NOESY NMR experiments (Supplementary Figure S1) combined with ^{1}H NMR analysis of oligonucleotides carrying the m-tel24 sequence containing specific thymine-to-uracil substitutions (necessary to assign the methyl groups of the thymidines in the sequence, see Supplementary Figure S2) to verify that the here used conditions did not alter the peculiar structural features of m-tel24 G-quadruplex. The obtained ^{1}H NMR chemical shifts of m-tel24 G-quadruplex are reported in Supplementary Table S1. Overall, our results show that, under the used conditions, m-tel24 adopts a G-quadruplex structure with hybrid-1 type topology (Figure 2B), comprising G3:G21:G17:G9, G4:G10:G16:G22, G5:G11:G15:G23 quartets, whereby G3, G9, G15, G16 and G21 are in *syn* conformation along the *N*-glycosidic bond and the other residues exhibit *anti* conformation. The core of the structure is connected by one propeller and two lateral T-T-A loops, while the 5′- and 3′-ends comprise T1-T2 and A24 flanking residues, respectively (Figure 2B). In this regard, m-tel24, studied herein at 100 mM KCl, exhibits the same structural features as previously reported at 70 mM KCl (35).

Before studying the interaction of **NDI-5** with both G-quadruplex models, the ligand alone was analyzed in solution by NMR. **NDI-5** ^{1}H NMR signals (Supplementary Figure S3) were assigned by means of 2D NMR experiments (Supplementary Figure S4). Similarly to other structurally related NDIs (24), under the studied neutral pH conditions, **NDI-5** is likely to be in its dicationic form (Supplementary Figure S4A). Interestingly, among the exchangeable protons of the free ligand, i.e. 4, 9, 18 and 19, only 4 was observed (at δ 10.02 ppm, see Supplementary Figure S3). This can be attributed to the intramolecular hydrogen bond with the close imide oxygen atom, with which proton 4 can form a stable 6-membered cyclic structure (Supplementary Figure S4A). Noteworthy, the ^{1}H NMR spectra of **NDI-5** did not show any detectable change if recorded on freshly prepared or aged samples, thus confirming the chemical stability of **NDI-5** in solution over time (Supplementary Figure S5).

*NMR study of the interactions between **NDI-5** and M2 G-quadruplex.* The interaction between M2 G-quadruplex and **NDI-5** was monitored by ^{1}H NMR titration experiments. Upon addition of 0.5 molar equivalents of **NDI-5**, broadening of the ^{1}H NMR imino signals corresponding to the free M2 G-quadruplex was observed, as well as appearance of new broad signals in the range of δ 10.67–10.78 ppm (Figure 3).

Further **NDI-5** additions up to 1:2 DNA:ligand ratio resulted in sharpening of the signals in the δ region 10.67–10.78 ppm and appearance of an additional signal at δ 11.13 ppm. At 1:3 DNA:ligand ratio twelve imino signals were resolved, corresponding to G-quadruplex/**NDI-5** complex, while the signals of free M2 G-quadruplex were no longer observed. The new set of twelve imino ^{1}H NMR signals appearing at 1:3 DNA:ligand ratio was shifted upfield with respect to the signals of free M2 G-quadruplex, indicating the formation of defined M2/**NDI-5** complexes (Figure 3). Only moderate shifts in the ^{1}H NMR imino signals were observed upon increasing the DNA:ligand ratio from 1:3 to 1:6, while further addition of **NDI-5** induced signal broadening again, whereby at 1:10 DNA:ligand ratio signals were hardly detectable from the baseline (Figure 3). Similar behaviour—i.e. ^{1}H NMR signals broadening upon addition from 0.5 to 2 eq. of **NDI-5**, sharpening from 3 to 6 eq. and broadening from 7 to 10 eq.—was observed in the aromatic, anomeric and methyl regions of the oligonucleotide (Supplementary Figures S6–S8). Moreover, at 0.2 mM DNA concentration and 1:7 DNA:ligand ratio, a precipitate formed in the NMR tube. No ^{1}H NMR spectral changes were observed upon monitoring the sample at 1:6 M2:**NDI-5** ratio for several weeks, indicating that the complexes obtained during the titration experiments were stable over a long time (Supplementary Figure S9). Severe broadening of ^{1}H NMR signals was observed for the sample at 1:6 M2:**NDI-5** ratio upon lowering the temperature from

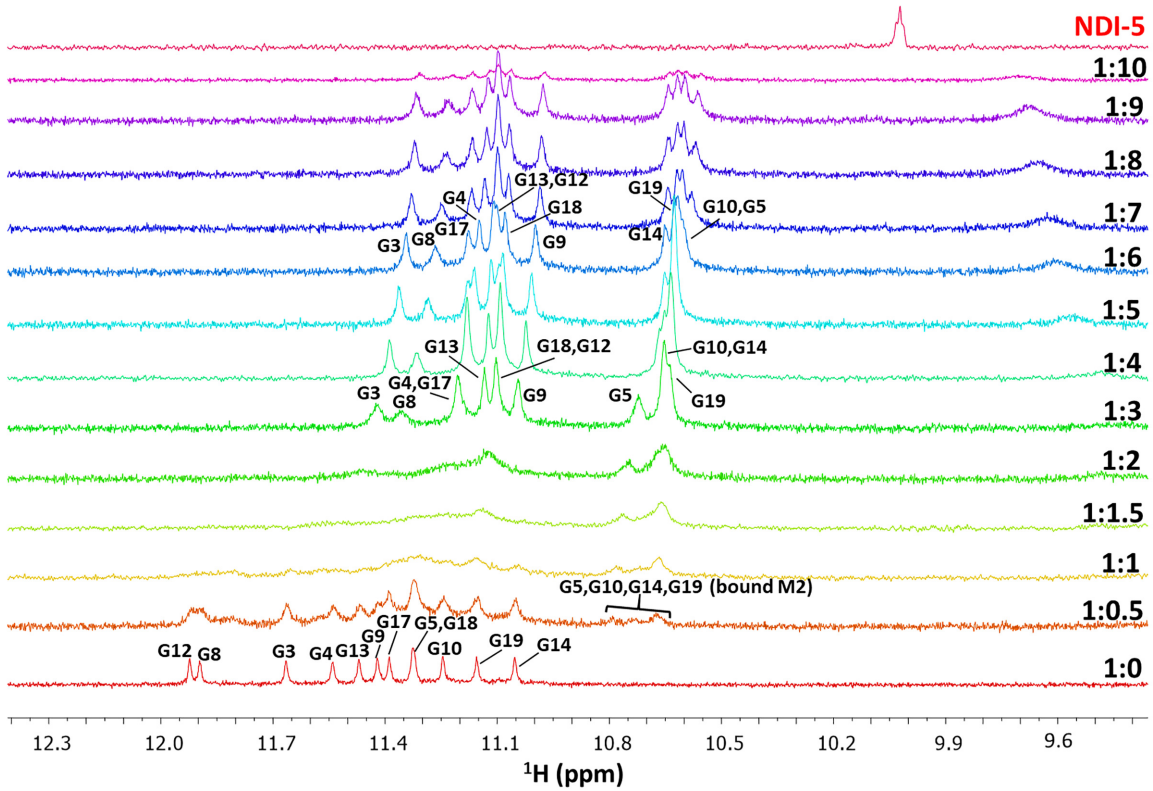

Figure 3. Imino regions of the ^{1}H NMR spectra of M2 G-quadruplex upon titration with **NDI-5** (from 0.5 to 10 equivalents). M2:**NDI-5** ratios are shown on the right of the corresponding spectrum. The NMR spectra were recorded in 90%/10% H_2O/D_2O at 0.2 mM DNA, 100 mM KCl, 20 mM potassium phosphate buffer (pH 7) and 25°C. Resonances for free M2 G-quadruplex are assigned according to ref. (34). On top, NMR spectrum of free **NDI-5** is reported, recorded in 90%/10% H_2O/D_2O at 0.2 mM NDI, 100 mM KCl, 20 mM potassium phosphate buffer (pH 7) and 25°C.

25 to 0°C (Supplementary Figure S10), consistent with the presence of different complexes at equilibrium of M2 G-quadruplex with **NDI-5**.

In order to get a deeper insight into the interactions between M2 G-quadruplex and **NDI-5**, 2D NMR experiments were performed on the samples at two different DNA/ligand ratios, i.e.: (i) 1:3, where the complete set of twelve ^{1}H NMR signals corresponding to M2 G-quadruplex/**NDI-5** complexes firstly resolved and (ii) 1:6, the highest ratio that could be explored in solution, considering that, at higher ligand concentration, sample precipitation occurred.

To unambiguously assign ^{1}H NMR resonances for 1:3 and 1:6 M2:**NDI-5** ratio samples, residue-specific ^{15}N- and ^{13}C-labelled M2 oligonucleotides were synthesized and analyzed by ^{15}N- and ^{13}C-HSQC experiments (Supplementary Figures S11-S18). ^{1}H NMR chemical shifts of M2 G-quadruplex in the absence and presence of 3 or 6 molar equivalents of **NDI-5** are reported in Supplementary Tables S2–S4. Addition of 3 molar equivalents of **NDI-5** triggered changes in ^{1}H NMR chemical shifts of M2 G-quadruplex, with the most prominently affected imino protons corresponding to G5, G10, G14 and G19 of the 3′-end quartet of M2 G-quadruplex, and to G8 and G12 of the 5′-end quartet (Figures 3 and 4). Interestingly, the same trend in ^{1}H NMR chemical shift perturbations of imino protons was observed at 1:6 M2:**NDI-5** ratio, i.e. the chemical shift differences observed upon addition of **NDI-5** were larger, intermediate and smaller for guanines of the 3′-end quartet, of the middle quartet and of the 5′-end quartet, respectively, with the only exception of G8 and G12 (Figure 4). Notably, lower chemical shift differences observed for G3 and G17 when compared to G8 and G12 in the upper quartet could be attributed to the presence of T1 and A2 flanking residues, partly shielding G3 and G17, which in turn renders G8 and G12 more accessible to ligand binding.

Considering the aromatic, methyl and H1′/H2′ sugar protons, the highest changes in ^{1}H NMR chemical shifts upon addition of **NDI-5** occurred at T1, A2 and T20 residues (Supplementary Figures S19 and S20). Interestingly, the chemical shift differences for aromatic and methyl protons were positive for T1 and negative in the case of A2 and T20, indicating that **NDI-5** binding to M2 G-quadruplex promotes π–π interactions of T1 coupled with repositioning of A2 and T20, which in turn exhibit weaker stacking to nearby G-quartets. These results are consistent with binding of **NDI-5** to both the 5′- and 3′-end quartets, thus perturbing the original stacking interactions of flanking segments on the two external G-quartets. Interestingly, new resolved ^{1}H NMR signals appearing upon addition of 0.5 molar equivalents of **NDI-5** corresponding to the bound form of M2 G-quadruplex are those of G5, G10, G14 and G19 in the imino region (Figure 3) and T20 in the methyl region (Supplementary Figure S8). Notably, however, analysis of the ^{1}H NMR signals at the low M2:**NDI-5** ratio showed that binding of **NDI-5** plausibly occurs to both 5′- and 3′-

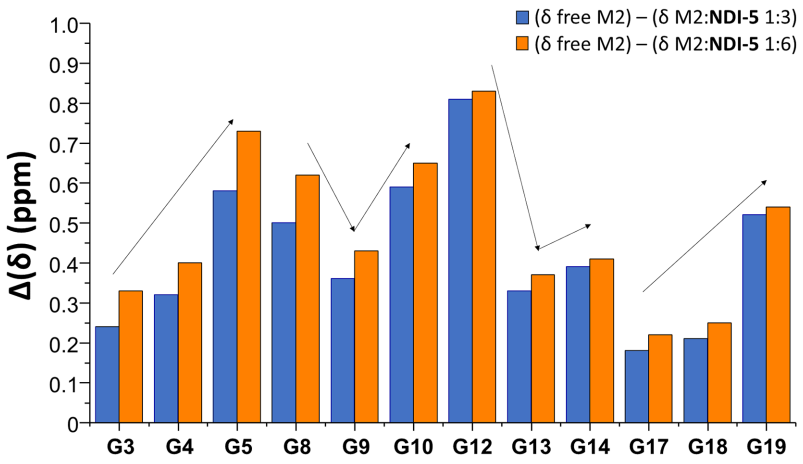

Figure 4. ^{1}H NMR chemical shift differences for imino protons of M2 G-quadruplex in the presence of 3 (blue bars) or 6 (orange bars) molar equivalents of **NDI-5** with respect to free M2 G-quadruplex. The errors associated with chemical shift differences are within ±0.05 ppm.

end quartets of M2 G-quadruplex. Assuming a stoichiometry of binding of 1:3, the NMR data indicate that the first binding events involve stacking of the aromatic core of **NDI-5** on the 5′- and 3′-end quartets (Figure 5A and B), while third binding comprises several different poses including binding to outer G-quartets (Figure 5C and D) and to A6-C7 (Figure 5E) and C15-A16 loops (Figure 5F). Binding in proximity of the one-residue loop C11 and/or the loop-free groove at G3, G4, G17 and G18 may not be favoured or at least is less important if considering the perturbations in the aromatic ^{1}H NMR chemical shifts upon titration experiments.

Interesting data were obtained by analysing increasing dilutions of 1:6 M2:**NDI-5** ratio sample prepared at 0.2 mM DNA concentration. In these experiments, ^{1}H NMR resonances progressively shifted downfield, approaching the chemical shift values, signals shape and resolution similar to that of 1:3 M2:**NDI-5** ratio sample, thus further supporting formation of the 1:3 complex (Supplementary Figure S21). The NMR results show that, at higher than 1:3 DNA:ligand ratios, the species comprising M2 G-quadruplex with three bound ligand molecules represents a platform for additional binding events in which **NDI-5** from bulk solution tends to interact with DNA or pre-bound ligand molecules in a 'ligand-shell' manner (*vide infra* for results of complementary methods). Upon dilution of the 1:6 system, **NDI-5** molecules are progressively released from the DNA/ligand complexes, resulting in M2:**NDI-5** complexes featuring three bound **NDI-5** molecules (Figure 5C-F). Inspection of the differences in ^{1}H NMR chemical shifts corresponding to G-quadruplex/**NDI-5** complexes at 1:6 versus 1:3 ratios showed the highest differences for imino protons of G3, G4, G5, G8, G9 and G10 and for aromatic and/or methyl protons of T1, A6, G9, G12 and A16 (Supplementary Figures S22 and S23). These findings suggested that the bound **NDI-5** molecules released upon dilution are localized close to the 5′-end and the A6-C7 and C15-A16 loops (Figure 5G–J).

Upfield shifts of ^{1}H NMR signals of imino and aromatic protons for all residues except T1 and T20 were observed upon increasing the DNA:**NDI-5** ratio from 1:3 to 1:6. Notably, negative differences in chemical shift changes for H6 and methyl protons of T1 indicate that binding of the additional ligand molecules promotes de-stacking of T1. On the other hand, T20 was not significantly affected by further addition of **NDI-5**, which indicates that no additional binding occurred at the 3′-end upon increasing the M2:**NDI-5** ratio from 1:3 to 1:6. Moreover, the binding of additional **NDI-5** molecules caused opposite perturbations in chemical shifts at DNA:ligand ratios higher than 1:3 with respect to the trend observed on going from 1:0 to 1:3 M2:**NDI-5** ratio for T1, A2, G5 and G19 residues, indicating that T1 was less involved, while A2, G5 and G19 were more involved in π-π stacking interactions at 1:6 than 1:3 M2:**NDI-5** ratio. These findings are consistent with multiple and mutually dependent binding events, which differently affect M2 G-quadruplex as a function of the **NDI-5** concentration, with ligand excess orchestrating the nucleotide residue rearrangement within the overall G-quadruplex structure.

Diffusion ordered spectroscopy (DOSY) experiments were performed on M2 G-quadruplex in absence and presence of 3, 6 and 9 equivalents of **NDI-5** (Supplementary Figures S24-S26). DOSY experiments at 9 molar equivalents of **NDI-5** were performed at 0.1 mM DNA concentration, thus avoiding precipitation phenomena. A translation diffusion coefficient (D_t) of 1.5 (± 0.1) × 10^{-10} $m^2 \cdot s^{-1}$ was obtained for both the free M2 G-quadruplex and G-quadruplex/ligand samples containing 3 and 9 **NDI-5** molar equivalents, and of 1.4 (± 0.1) × 10^{-10} $m^2 \cdot s^{-1}$ for the G-quadruplex/ligand sample including six **NDI-5** molar equivalents. From the D_t values found for the M2 G-quadruplex alone, calculations based on a spherical model (39) provided a hydrodynamic diameter of 3.2 (±0.2) nm (including the hydration layer of 2 × 0.28 nm (42)), which is in full agreement with the value predicted by HYDROPRO software (43) (3.2 nm) for M2 G-quadruplex (PDB entry 5NYS) (34). Similar hydrodynamic diameter values were derived for M2 G-quadruplex in the presence of 3, 6 and 9 molar equivalents of **NDI-5**, i.e. 3.2 (±0.2) nm for the 1:3 and 1:9, and 3.4 (±0.2) nm for the 1:6 system. Overall, these findings indicate that the M2 G-quadruplex retains a monomeric fold even when bound to the ligand.

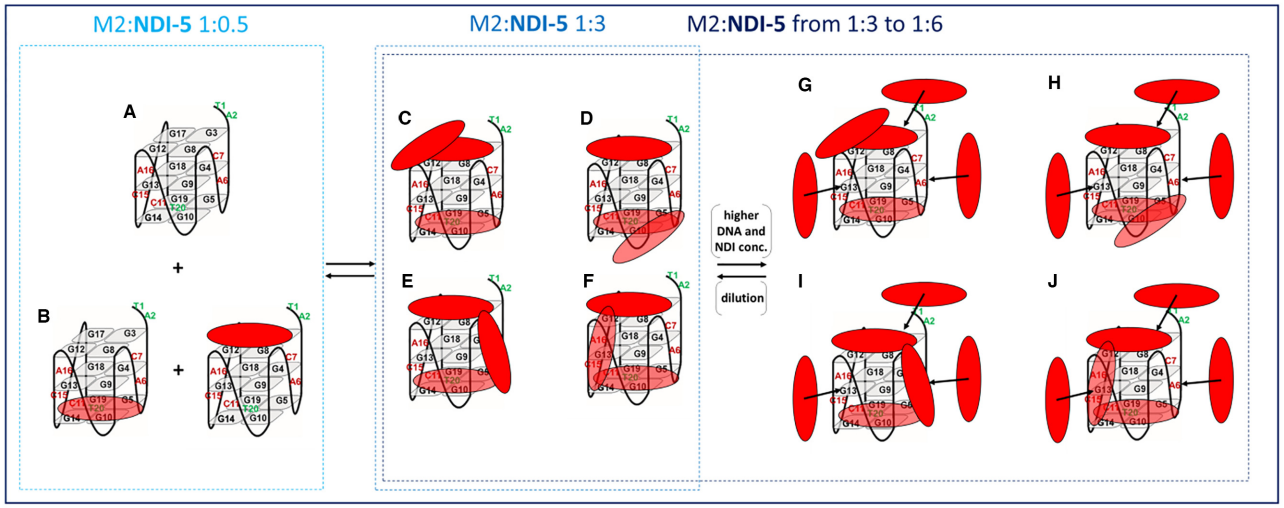

Figure 5. Schematic representation of the binding poses involved in the M2/**NDI-5** complex formation, as inferred from NMR experiments. Free M2 and 1:1 M2/**NDI-5** complex formed upon titrating M2 up to 1:0.5 M2/**NDI-5** ratio are represented in (**A**) and (**B**), respectively. Putative 1:3 and 1:6 M2/**NDI-5** complexes are depicted in (**C**)–(**F**) and (**G**)–(**J**), respectively.

For the **NDI-5**-containing systems, the absence of substantial changes in M2 G-quadruplex hydrodynamic dimensions compared to the free M2 G-quadruplex could be explained assuming that the overall G-quadruplex structure is rendered more compact and stiff upon binding, thus compensating the increase in size due to the ligand complexation.

Additionally, 2D NMR experiments, i.e. NOESY (Supplementary Figures S27 and S28) and TOCSY (Supplementary Figure S29) experiments, were performed on 1:3 and 1:6 M2:**NDI-5** ratio samples in order to assign ^{1}H NMR signals and characterize the interactions between M2 G-quadruplex and **NDI-5**. Higher resolution together with a higher number of NOE cross-peaks for the 1:6 M2:**NDI-5** system in comparison to the 1:3 one demonstrated that saturating the complex with a ligand excess was beneficial for the spectroscopic characterization. The position of the ligand at both external G-quartets was supported by several DNA/**NDI-5** intermolecular NOE cross-peaks summarized in Supplementary Table S5. Moreover, intermolecular **NDI-5**/**NDI-5** interactions are sustained by a number of NOE cross-peaks between protons of different **NDI-5** molecules (Supplementary Table S6). However, the intermolecular **NDI-5**/**NDI-5** NOE cross-peaks were observed with very low intensities and only at mixing time of 500 ms. While broadening of ^{1}H NMR signals precluded structural insights at low temperatures (Supplementary Figure S10), progressive heating of the 1:6 M2:**NDI-5** ratio sample from 25 to 50°C allowed sharpening the ^{1}H NMR signals, enabling more detailed analysis (Supplementary Figures S30 and S31). Notably, **NDI-5**/**NDI-5** NOE cross-peaks resolved at 50°C (Supplementary Figure S32), thus allowing inspection of the interactions among **NDI-5** molecules. This extended the details observed at 25°C, in particular the intermolecular interactions of the ligands aromatic protons and different pendant groups, altogether demonstrating equilibrium of different **NDI-5**/**NDI-5** interacting modes. Finally, on the basis of this assignment of **NDI-5** protons in the complexes with M2 G-quadruplex, differences in chemical shifts between free and bound **NDI-5** were calculated and reported in Supplementary Figure S33. All **NDI-5** protons were significantly perturbed upon binding ($(\Delta\delta)_{\text{free-bound}} > 0.05$ ppm) indicating that the interaction with M2 G-quadruplex affected the whole ligand molecule.

Eventually, the ability of **NDI-5** to induce the formation of G-quadruplex structures starting from unfolded M2 oligonucleotide was evaluated. Interestingly, upon addition of 6 molar equivalents of **NDI-5** to the oligonucleotide dissolved in a metal cation-free solution, new broad signals in the range of δ 10.56–11.10 ppm appeared (Supplementary Figure S34). This result indicates that **NDI-5** induces formation of G-quadruplex structures in absence of stabilizing K^+ ions, with different DNA-ligand complexes in equilibrium among them.

*NMR study of the interactions of **NDI-5** with modified M2 G-quadruplexes containing abasic sites in the loops.* In order to investigate the role of the A6-C7 and C15-A16 loop residues in the interaction of M2 parallel G-quadruplex with **NDI-5**, we synthesized modified M2 oligonucleotides containing natural-to-abasic residue modifications in the first loop (M2-L1), in the third (M2-L3) or in both loops (M2-L1L3) (Supplementary Figure S35). Notably, G-quadruplexes containing natural-to-abasic residues substitutions in loop regions were expected to maintain the original parallel folding topology (44). Considering that C11, comprised in the second loop, exhibited only minor ^{1}H NMR chemical shift perturbations upon titration experiments, and that no NOE correlations were observed between C11 and **NDI-5**, the M2 analogue with natural-to-abasic substitution in the second loop was not included in our study. Inspection of NMR parameters and in particular comparison of ^{1}H NMR chemical shifts, DOSY-derived hydrodynamic diameters and NOE correlations for the M2-L1, M2-L3 and M2-L1L3 with respect to M2 demonstrated that all the modified oligonucleotides in the presence of K^+

ions adopted monomeric G-quadruplex folds with similar structural features as the parent M2. Notably, relevant ^{1}H chemical shift differences (i.e., $\Delta\delta > 0.05$ ppm) between the M2 G-quadruplex and the modified analogues were found only for imino signals of G4 and G13 and aromatic signals of G5, G8 and G9, in addition to loop sugar protons (Supplementary Figures S36-S38). However, careful comparative analysis of hydrodynamic diameters (Supplementary Table S7) and NOE connectivities (Supplementary Figure S39) for M2-L1, M2-L3 and M2-L1L3 with respect to M2 indicated that all these models shared common structural properties.

Titrations of M2-L1, M2-L3 and M2-L1L3 with **NDI-5** monitored by ^{1}H NMR analysis (Supplementary Figures S40–S48) resulted in gradual appearance of twelve well-resolved imino protons corresponding to G-quadruplex/ligand complexes in each case. The imino ^{1}H NMR signals corresponding to these complexes were upfield shifted with respect to the signals of the free G-quadruplexes and appeared at 1:4, 1:4 and 1:3 G-quadruplex/ligand ratios for M2-L1, M2-L3 and M2-L1L3, respectively. Interestingly, narrowing of ^{1}H NMR signals in the case of M2-L1 and M2-L3 occurred upon addition of one additional molar equivalent of **NDI-5** with respect to M2-L1L3 and M2, i.e. 1:4 versus 1:3 DNA:ligand ratio, suggesting for the latter cases an interesting role of the nucleobases of the loops in the binding events. We interpret these differences in the ^{1}H NMR spectra upon **NDI-5** titration experiments considering the presence of four putative binding sites on each G-quadruplex, hereafter named *A*, *B*, *C* and *D*. *A* and *B* correspond to the first **NDI-5** binding sites at the 5'- and 3'-end quartets (see Figure 5B) for all the investigated M2, M2-L1, M2-L3 and M2-L1L3 G-quadruplexes. In the case of M2 as well as of M2-L1L3, binding to *C* (see 1:3 M2:**NDI-5** complexes in Figure 5C–F) is favoured with respect to *D*, which is not occupied by **NDI-5** at 1:3 DNA:ligand ratio and may correspond to the binding site(s) where **NDI-5** interacts through pre-bound **NDI-5** (see 1:6 M2:**NDI-5** complexes in Figure 5G–J). Regarding M2-L1 and M2-L3, the presence of abasic residues imposes similar binding affinities of **NDI-5** to *C* and *D*, so that binding site preference for **NDI-5** is as follows: $A = B > C = D$. Moreover, observation of ^{1}H NMR signal sharpening at 1:4 rather than 1:3 DNA:ligand ratio in case of M2-L1 and M2-L3 is consistent with the equilibrium among species exhibiting **NDI-5** bound to *A, B, C* and *A, B, D*, which is intermediate on the NMR time scale at both 600 and 800 MHz. Furthermore, the fact that the M2-L1L3 G-quadruplex, containing abasic residues in two loops, shows similar **NDI-5** binding profiles as the parent M2 G-quadruplex suggests that the nucleobases in the loops connecting the core of the structure do not crucially impede binding, but may orchestrate the dynamics of DNA remodelling in the sequential ligand binding.

The analysis of ^{1}H NMR chemical shift differences for imino, aromatic, methyl and sugar protons corresponding to M2-L1, M2-L3 and M2-L1L3 in the absence or presence of 6 molar equivalents of **NDI-5** revealed that changes induced by **NDI-5** binding are similar as for M2 (Supplementary Figures S49-S51), consistent with **NDI-5** interacting similarly with all the investigated G-quadruplexes. Moreover, DOSY experiments proved that the overall size, and thus the monomeric G-quadruplex fold was preserved for M2-L1, M2-L3 and M2-L1L3 even after **NDI-5** binding (Supplementary Table S7). To get a deeper insight into the binding mode of **NDI-5** towards the modified M2 oligonucleotides, 2D-NOESY spectra were recorded for M2-L1, M2-L3 and M2-L1L3 G-quadruplexes in the presence of 6 molar equivalents of **NDI-5**, showing similar sequential correlations as M2 (Supplementary Figure S52). Interestingly, NMR spectra of the investigated G-quadruplexes in the presence of 6 molar equivalents of **NDI-5** revealed two signals at ca. δ 6.8 and 7.0 ppm for M2 (Supplementary Figure S53), whereby in the case of M2-L1, M2-L3 and M2-L1L3 only the former, only the latter or no signal was observed respectively, suggesting that these signals were diagnostic for **NDI-5** interaction with the loops. Additionally, analysis of intermolecular NOE cross-peaks between **NDI-5** and all the investigated G-quadruplexes (Supplementary Tables S5 and S8) revealed similarities among all the studied complexes. Moreover, almost all the contacts between different **NDI-5** molecules are common to M2-L1, M2-L3 and M2-L1L3 (as well as M2) G-quadruplexes at 1:6 DNA:ligand ratio (Supplementary Table S9). Finally, analysis of ^{1}H NMR chemical shift differences between free and bound **NDI-5** in 1:6 DNA:ligand ratio samples showed that the systems comprising M2-L1, M2-L3 and M2-L1L3 had an essentially similar behaviour as M2. Additionally, the analysis of ^{1}H NMR chemical shift perturbations upon ligand binding revealed the following trend in terms of the differences between free and bound **NDI-5**: M2-L1 $\geq$ M2-L3 $>$ M2-L1L3 $\geq$ M2 (Supplementary Figure S54). The consistently higher similarity in ^{1}H NMR chemical shifts of bound **NDI-5** in case of M2-L1L3 to the parent M2 in comparison to M2-L1 and M2-L2 indicates that, albeit subtly, A6-C7 and C15-A16 loop regions modulate the ligand binding mutually. Therefore, it can be concluded that in all cases the interaction with the investigated G-quadruplexes involves the whole ligand molecules and **NDI-5** is more perturbed upon binding to M2-L1 and M2-L3 than to M2-L1L3 and M2. These data provide further confirmation that the most similar complexes to those found with the unmodified M2 G-quadruplex are the ones formed with M2-L1L3 G-quadruplex.

*NMR study of the interactions between **NDI-5** and m-tel24 G-quadruplex.* Titration of m-tel24 G-quadruplex with **NDI-5**—performed under the same conditions used for M2 G-quadruplex, i.e. at 100 mM KCl and 20 mM potassium phosphate buffer (pH 7.0)—showed a stepwise broadening of the signals (Figure 6 and Supplementary Figure S55–S58).

In parallel, novel ^{1}H NMR signals of m-tel24 appeared in the imino region (Supplementary Figure S55) upon increasing **NDI-5** concentration. Notably, these signals were upfield shifted with respect to the free m-tel24 G-quadruplex and assigned to m-tel24/**NDI-5** complexes. The binding of **NDI-5** to m-tel24 was evident from dramatic line broadening of imino ^{1}H NMR signals even at 0.5 molar equivalents (Figure 6) with more pronounced effect observed for G3,

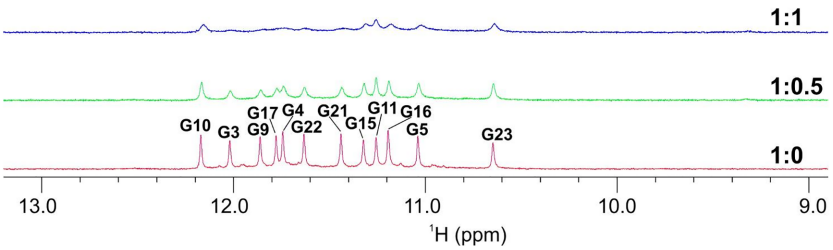

Figure 6. Imino regions of the ^{1}H NMR spectra of m-tel24 G-quadruplex upon titration with **NDI-5**. m-tel24:**NDI-5** ratios are shown on the right of the corresponding spectrum. The spectra were recorded in 90%/10% H_2O/D_2O at 0.2 mM DNA, 100 mM KCl, 20 mM potassium phosphate buffer (pH 7) and 25°C.

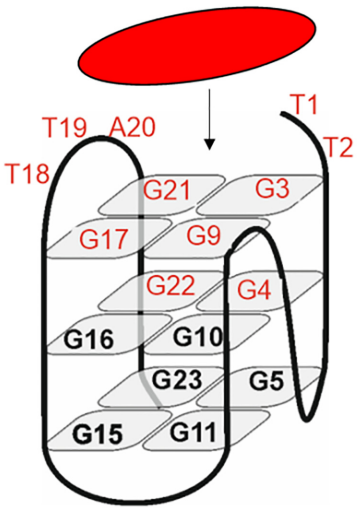

Figure 7. Depiction of the preferential binding site of **NDI-5** on m-tel24 G-quadruplex as inferred from NMR data. Residues exhibiting marked broadening of their ^{1}H NMR signals already at 1:0.5 DNA/**NDI-5** ratio are highlighted in red.

G4, G9, G17, G21 and G22 (Supplementary Figure S59). Notably, G3, G9, G17 and G21 compose the 5'-end quartet of m-tel24 G-quadruplex, while G4 and G22 are comprised in the middle G-quartet. Line broadening of ^{1}H NMR signals was also evident for the aromatic protons of G17, T19, A20 and G22 and methyl groups of T1, T2, T18 and T19 (Supplementary Figures S56 and S58). Overall, these findings point to a specific binding mode of **NDI-5** to m-tel24 G-quadruplex at the 5′-end, as schematically shown in Figure 7. However, even at higher **NDI-5** concentration, no sharpening of ^{1}H NMR signals was observed, denoting that complex equilibria, intermediate-to-fast on the NMR time scale, occurred. No change in ^{1}H NMR signals could be observed upon aging the sample at 1:6 m-tel24:**NDI-5** ratio for several weeks (Supplementary Figure S60). Interestingly, the number of ^{1}H NMR signals increased upon lowering the sample temperature from 25 to 0°C (Supplementary Figure S61), while several, especially aromatic ^{1}H NMR signals were more resolved at temperatures above 25°C (Supplementary Figures S62 and S63). Nevertheless, the spectral resolution and severity of line broadening at both lower and higher temperatures than 25°C did not warrant more detailed structural characterization. Notably, no precipitate formation was observed even at m-tel24:**NDI-5** 1:20 ratio. Overall, the observed behaviour suggests that **NDI-5** exhibits multiple binding poses on a single m-tel24 G-quadruplex unit and/or different m-tel24:**NDI-5** complexes comprising two or more G-quadruplex units could be formed. For the m-tel24:**NDI-5** system, the low intensity of the ^{1}H NMR signals in the imino as well as in the other spectral regions discouraged further, more in-depth NMR experiments.

Dynamic Light Scattering experiments

In order to measure the hydrodynamic diameter of DNA:**NDI-5** complexes, in addition to the DOSY experiments described in section 3.1.2, DLS analysis was carried out. In detail, aqueous solutions of M2 and m-tel24 G-quadruplexes were titrated with increasing amounts of **NDI-5** (up to 6 molar equivalents) and DLS analysis performed after equilibration of each sample (Figure 8). The volume-based particle size distribution showed the presence of a single species for both M2 and m-tel24 G-quadruplexes in the absence of ligand, with hydrodynamic diameter of 3.1 (±0.5) and 3.2 (±0.4) nm, respectively. No significant variation of hydrodynamic diameter for M2 G-quadruplex was observed upon addition of **NDI-5** (Figure 8A), in full agreement with DOSY experiments. As concerns m-tel24 titration, the addition of 1 molar equivalent of ligand led to the formation of m-tel24/**NDI-5** complexes with a diameter of 4.9 (±0.8) nm (Figure 8B), indicating a drastic change in size, which may correspond to species comprising two G-quadruplex units whose interaction is mediated by **NDI-5** molecules. Notably, the m-tel24/**NDI-5** complexes including 1 and 2 molar equivalents of **NDI-5** had the same size. From 3 to 6 molar **NDI-5** equivalents, species with even higher hydrodynamic diameter (average value = 7.3 nm) were observed, compatible with higher order G-quadruplex structures (Figure 8B). The results obtained for the m-tel24:**NDI-5** system showed different DNA/**NDI-5** complexes—comprising one, two or more G-quadruplex units—in equilibrium. Notably, these results are consistent with the above described NMR behaviour of the m-tel24:**NDI-5** system. Indeed, the ^{1}H NMR signal broadening for m-tel24:**NDI-5** system observed at ratios from 1:1 onwards can be well explained considering the formation of different m-tel24:**NDI-5** complexes comprising two or more G-quadruplex units which are involved in intermediate-to-fast equilibria on the NMR time scale.

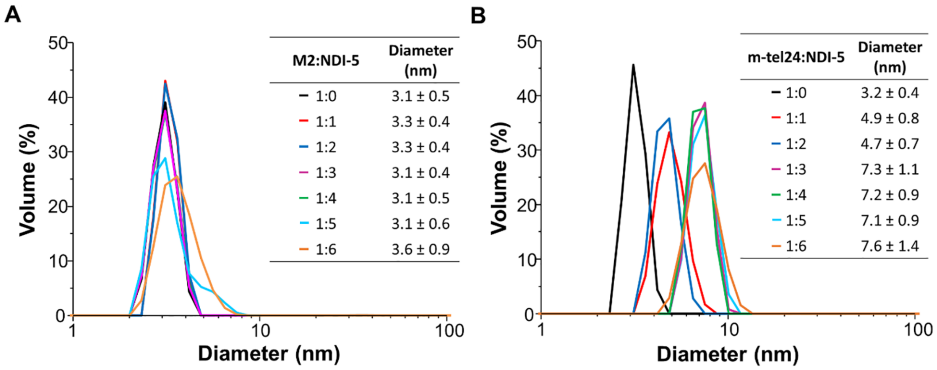

Figure 8. Volume-based particle size distribution for (**A**) M2 and (**B**) m-tel24 G-quadruplexes in the absence and presence of different amounts of **NDI-5** (up to 6 equivalents). DLS experiments were performed at 0.16 mM (for M2) or 0.13 mM (for m-tel24) DNA, 100 mM KCl, 20 mM potassium phosphate buffer (pH 7) and 25°C. Tables report the hydrodynamic diameters (±S.D.) for the different species formed on increasing **NDI-5** concentration.

Circular dichroism experiments

Circular dichroism experiments were carried out in the absence and presence of **NDI-5** to evaluate the effects of this ligand on the overall conformational behaviour of M2 and m-tel24. CD spectra showed that M2 folded into a parallel G-quadruplex, featured by a maximum at 265 nm and a minimum at 243 nm, while m-tel24 folded into a hybrid G-quadruplex, featured by a maximum at 290 nm and a shoulder at 270 nm (Figure 9A and B, respectively), confirming the expected conformations for these G-quadruplex structures under the explored solution conditions. Then solutions of M2 and m-tel24 G-quadruplexes were titrated with increasing amounts of **NDI-5** and CD spectra recorded after each addition. Upon titrating M2 G-quadruplex with **NDI-5**, reduction in the intensity of the 265 nm band was observed (Figure 9A). When m-tel24 was treated with **NDI-5**, a dose-dependent increase of the intensity of the 290 nm band occurred as well as a reduction of the 270 nm shoulder (Figure 9B). Thus, conformational changes were detected for both the investigated structures, proving that **NDI-5** somehow affected G-quartets and/or flanking segments stacking in both M2 and m-tel24 G-quadruplexes. However, the parallel fold was preserved for M2 G-quadruplex, while, interestingly, conformational changes were induced on m-tel24 G-quadruplex by the presence of **NDI-5**, plausibly indicating a switch from hybrid to antiparallel topology, similarly to what previously observed for titrations on parallel c-myc and hybrid tel26 G-quadruplexes (21).

CD-melting experiments were also performed to evaluate if stabilizing or destabilizing effects on the G-quadruplexes were obtained upon incubation with **NDI-5**. CD melting curves of M2 and m-tel24 in the absence or presence of the ligand (1:6 DNA:**NDI-5** ratio) were recorded by following the CD changes at the wavelength of intensity maximum (265 and 290 nm, respectively). The CD melting experiments (Supplementary Figure S64) showed T_m of 78 and 85 (±1) °C for M2, and T_m values of 61 and 74 (±1) °C for m-tel24, respectively in the absence or presence of 6 ligand equivalents, proving that **NDI-5** was able to produce stabilizing effects on both G-quadruplexes (ΔT_m = +7 and +13°C, respectively). Then, in order to evaluate the ability of **NDI-5** to induce the formation of G-quadruplex structures in both M2 and m-tel24 systems starting from the unfolded oligonucleotides in a metal cation-free buffer, additional CD experiments were carried out. In detail, a solution of unstructured m-tel24 oligonucleotide in Tris–HCl buffer (pH 7) was titrated with increasing amounts of **NDI-5**, and CD spectra recorded after each addition (Supplementary Figure S65A). Interestingly, **NDI-5** was able to induce structuring of the unfolded m-tel24 oligonucleotide, which formed an antiparallel G-quadruplex structure featured by a T_m value of 45°C (Supplementary Figures S65A and S65B, respectively). On the contrary, no data about the **NDI-5** ability to induce structuring of M2 could be gained, since this system proved to fold into a stable secondary structure, i.e. a parallel G-quadruplex, even in a metal cation-free buffer (Supplementary Figure S65C).

Fluorescence experiments

To get information about the binding stoichiometry and constants for the complexes formed between **NDI-5** and M2 or m-tel24 G-quadruplex, fluorescence experiments were carried out.

Fluorescence titration experiments were performed at a fixed concentration of ligand, by adding increasing amounts of each G-quadruplex. In detail, **NDI-5** solutions were titrated with increasing amounts of M2 or m-tel24 solutions, and the corresponding fluorescence spectra, after each addition, were recorded (Supplementary Figures S66A and B, respectively). A significant fluorescence quenching was observed in both titration experiments, further confirming the interaction between **NDI-5** and the G-quadruplex structures. The fraction of bound **NDI-5** was calculated from the obtained fluorescence intensity values and reported as a function of the DNA concentration (Figure 10A and B). In the absence of suitable mathematical models for an accurate description of complex systems including multiple binding events, data were fitted with one of the most validated models for the determination of G-quadruplex/ligand binding constants, i.e. the independent and equivalent-sites model (19,41). Considering the simplicity of the above model with respect to the complexity of our G-quadruplex/ligand systems, which – for their intrinsic asymmetry – cannot offer identical binding sites, the

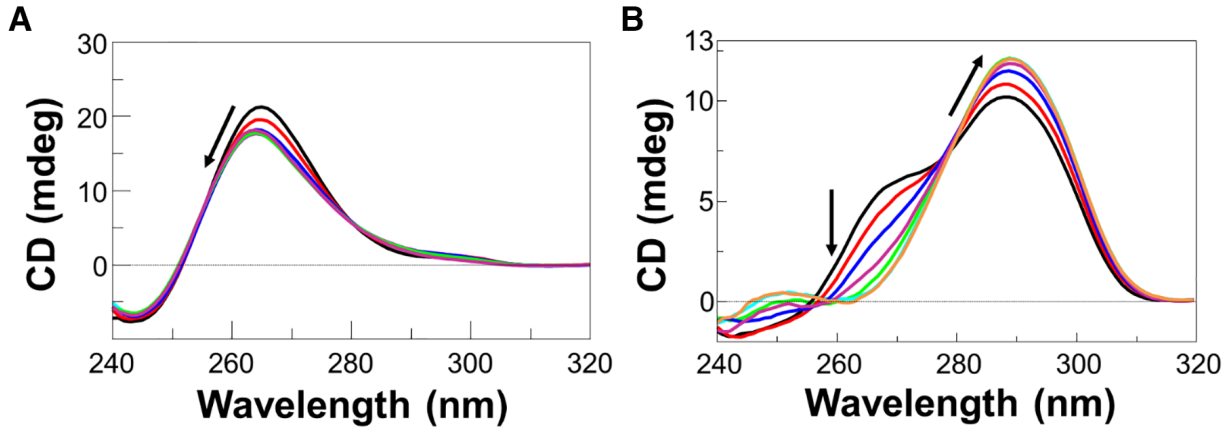

Figure 9. CD spectra of solutions of (**A**) M2 and (**B**) m-tel24 at 2 μM concentration at 20 mM KCl, 5 mM potassium phosphate buffer (pH 7) and 20°C, in the absence (black lines) and presence of increasing amounts of **NDI-5**. Black arrows indicate intensity variations of the specific bands going from 1:1 to 1:6 DNA:NDI ratios.

constants thus derived have to be considered only as apparent constants. In fact, as also well highlighted by other authors (45–47), formation of high stoichiometry complexes inevitably involves non-equivalent G4 binding sites of presumably different affinity, mostly unresolved when following fluorescence (and more generally spectroscopic) changes. Consequently, binding parameters resulting from fitting the isotherms of fluorescence titrations using a simplified model with n equivalent and independent binding sites should be considered only as rough estimates of real binding constants and stoichiometries. Thus, using this fitting, binding stoichiometries of 1:3 and 1:4 were found respectively for M2/**NDI-5** and m-tel24/**NDI-5** complexes. In addition, apparent binding constants of 2.4 (±0.9) × 10^7 and 7 (±1) × 10^6 M^{-1} (corresponding to apparent dissociation constants of 42±16 and 143±20 nM) were determined respectively for M2/**NDI-5** and m-tel24/**NDI-5**, thus proving the tight interaction of **NDI-5** with both G-quadruplexes. These data also indicated a moderate preference of the ligand for a parallel G-quadruplex.

Additionally, fluorescence spectra were also recorded to obtain the Job plots for different DNA/ligand mixtures, prepared by varying the **NDI-5** molar fraction from 0 to 1 and keeping constant the total molar concentration ([ligand] + [DNA]) (Supplementary Figures S66C and D). Even though their complete reliability when applied to complexes featured by high stoichiometries of binding is matter of debate (48,49), Job plots represent an independent method for the determination of binding stoichiometry, largely applied also in the recent literature (for example, see: 50–52). The analysis of the Job plot for M2/**NDI-5** mixtures showed a unique drastic change at **NDI-5** molar fraction of 0.76, corresponding to 1:3 stoichiometry ratio for the M2:**NDI-5** complex (Figure 10C). This result, in excellent agreement with the data determined by the fluorescence titration fitting and the ^{1}H NMR titration for the parallel G-quadruplex model, provides an additional and independent evidence in support of the 1:3 binding stoichiometry for the M2:**NDI-5** complex. On the other hand, Job plot analysis for m-tel24/**NDI-5** mixtures showed changes at **NDI-5** molar fractions of 0.65 and 0.80, corresponding to stoichiometries of approximately 1:2 and 1:4 m-tel24:**NDI-5** (Figure 10D), thus evidencing two consecutive binding events in which, for each of these, two distinct **NDI-5** molecules—or a dimer of **NDI-5** – bind the hybrid G-quadruplex model.

CONCLUSIONS

Naphthalene diimides are increasingly emerging as attractive, putative anticancer drugs due to their well-proven ability to bind cancer-related G-quadruplex structures (22–26). Recently, a new trifunctionalized G-quadruplex-targeting naphthalene diimide, named **NDI-5**, was discovered to have a selective antitumor activity in vitro in the low nM range, showing potential as a promising lead compound to develop future candidate drugs for *in vivo* studies (21). Despite the wide interest in this class of compounds as G-quadruplex ligands, to the best of our knowledge no in-depth NMR study on the interactions of naphthalene diimides with G-quadruplexes in solution had been carried out thus far.

Here, we reported the first extensive NMR study on the interaction of a naphthalene diimide—the trifunctionalized **NDI-5**—with G-quadruplex models adopting different topologies, i.e. a parallel-type (M2) and a hybrid-type (m-tel24) structure (34,35). To complement the NMR data, dynamic light scattering, circular dichroism and fluorescence analyses were also performed. This work provided details on the binding of this dicationic, trifunctionalized naphthalene diimide with model G-quadruplexes of parallel and hybrid type, characterized by interplay of different binding modes. **NDI-5** was found to induce hybrid-to-antiparallel conformational changes in m-tel24, in turn not significantly altering the parallel G-quadruplex structure of M2. Upon binding, **NDI-5** produced marked stabilizing effects on both G-quadruplexes ($\Delta T_m \geq +7$°C). From fluorescence titration experiments, apparent dissociation constants of 42 and 143 nM were determined respectively for M2/**NDI-5** and m-tel24/**NDI-5** complexes, indicative of the high affinity of this ligand for both G-quadruplexes, but with some preference for the parallel topology.

As concerns M2 G-quadruplex, its monomeric fold was preserved upon ligand binding, with formation of com-

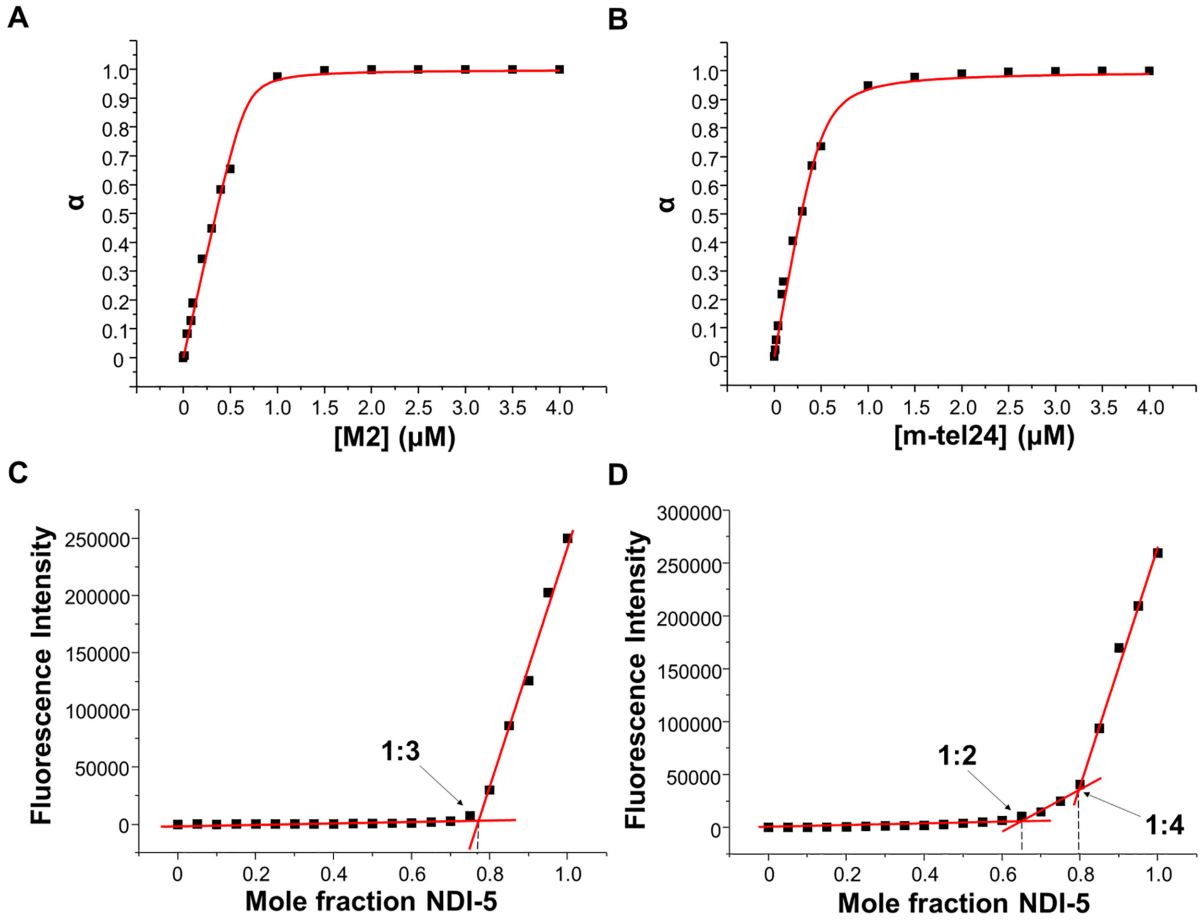

Figure 10. (**A**) and (**B**): Fluorescence titration experiments. Representative binding curve obtained by plotting the fraction of bound ligand **NDI-5** (α) as a function of A) M2 and B) m-tel24 concentration. The black squares represent the experimental data; the red line is the best fit obtained with an independent and equivalent-sites model. (**C**) and (**D**): Job plot analysis for the binding of **NDI-5** to M2 and m-tel24, respectively. The total molar concentration ([ligand] + [DNA]) was kept constant at 2 μM. The black squares represent the experimental data of a single replicate. The fluorescence experiments were performed at 20 mM KCl, 5 mM potassium phosphate buffer (pH 7) and 20°C. The excitation and emission wavelengths were 526 and 589 nm, respectively.

plexes characterized by binding stoichiometry of 1:3. **NDI-5** preferentially bound M2 at the lower quartet and the 3′-end close residues, as well as at the upper quartet and the 5′-end close residues, in turn perturbing the stacking interactions of flanking nucleotides on the two external G-quartets of M2 G-quadruplex. The M2 loops containing two nucleobases proved to mediate the interaction between **NDI-5** and the G-quadruplex. Conversely, the M2 loop containing a single residue was not involved in the ligand complexation. While direct stacking of the ligand on G-quartet surfaces appeared decisive for the interaction, the role of loops was notable in the context of interdependence of the secondary binding events: indeed, **NDI-5** binding could be coupled with induced stacking interactions within A6-C7 and C15-A16, not accessible in the one-residue C11 loop. The binding of **NDI-5** at the 5′-end of the parallel G-quadruplex included participation of T1 and A2 terminal residues, in agreement with previously resolved crystal structures of naphthalene diimides-G-quadruplexes complexes (25,53,54). Notably, the ligand core, with its rigid skeleton, could provide the main interface for NDI binding to a G-quadruplex via end-stacking mode, whereas the more flexible pendant groups offered the possibility of finely tuning the binding, also depending on the overall shape and nature of the loops. Interestingly, when abasic sites were introduced in A6-C7 and/or C15-A16 M2 G-quadruplex loops, the M2 G-quadruplex with abasic sites in both loops was the most similar to unmodified M2 in **NDI-5** binding behaviour. This indicates that modifications at the level of a single propeller loop introduce changes in the overall symmetry of the M2 G-quadruplex structure that can be compensated upon insertion of abasic residues in two opposite propeller loops. Then, it has to be considered that not only the structural, but also the dynamic aspect of the interaction, in particular the targeted structure breathing, is crucial for the binding affinity and specificity of the ligand.

In the case of m-tel24 G-quadruplex, ^{1}H NMR signal broadening observed for the complexes with **NDI-5** suggested that multiple binding poses of the ligand on a single G-quadruplex unit and/or different complexes, comprising two or more G-quadruplex units, could be formed when targeting hybrid G-quadruplexes. DLS results confirmed these hypotheses, showing the formation of DNA/ligand higher-order species upon increasing the **NDI-5** concentration.

In summary, although several binding sites and stoichiometries were observed with both M2 and m-tel24 G-

quadruplexes, both models showed preferential binding of **NDI-5** at the outer G-quartets, with the initial binding events occurring at both 5′- and 3′-ends in the case of the parallel G-quadruplex and at the 5′-end for the hybrid G-quadruplex. This behaviour could be explained considering the high propensity of **NDI-5** to interact with G-quadruplex targets mainly by stacking interactions. On this basis, the different degree of accessibility of the planar aromatic surfaces of G-quadruplex structures seems to be the main structural element directing **NDI-5** binding preferences. Overall, this structural investigation will be helpful for the future design of optimized **NDI-5** analogues as effective candidate drugs in anticancer targeted therapies, allowing the construction of reliable models for the G-quadruplex/**NDI-5** complexes in docking studies aimed at the development of second-generation optimized NDI derivatives.

DATA AVAILABILITY

Biological Magnetic Resonance Data Bank ID: 50378.

SUPPLEMENTARY DATA

Supplementary Data are available at NAR Online.

ACKNOWLEDGEMENTS

The authors acknowledge the CERIC-ERIC consortium for access to NMR facilities.

FUNDING

C.P. was financially supported by UniNA and Compagnia di San Paolo, in the frame of 'Programma STAR, and by a FIRC-AIRC fellowship for Italy; Slovenian Research Agency [P1-0242, J1-1704, J3-7245, J7-9399]. Funding for open access charge: University of Napoli, Department of Chemical Sciences.
Conflict of interest statement. None declared.

REFERENCES

1. Fitzmaurice,C. (2017) Global, regional, and national cancer incidence, mortality, years of life lost, years lived with disability, and disability- adjusted life-years for 32 cancer groups, 1990 to 2015: a systematic analysis for the global burden of disease study. *JAMA Oncol.*, **3**, 524–548.
2. Chakraborty,S. and Rahman,T. (2012) The difficulties in cancer treatment. *eCancer*, **6**, 1–5.
3. Ruden,M. and Puri,N. (2013) Novel anticancer therapeutics targeting telomerase. *Cancer Treat. Rev.*, **39**, 444–456.
4. Tsimberidou,A.-M. (2015) Targeted therapy in cancer. *Cancer Chemother. Pharmacol.*, **76**, 1113–1132.
5. Xu,Y. and Goldkorn,A. (2016) Telomere and telomerase therapeutics in cancer. *Genes (Basel)*, **7**, 22.
6. Shalaby,T., Fiaschetti,G., Nagasawa,K., Shin-Ya,K., Baumgartner,M. and Grotzer,M. (2013) G-quadruplexes as potential therapeutic targets for embryonal tumors. *Molecules*, **18**, 12500–12537.
7. Hänsel-Hertsch,R., Spiegel,J., Marsico,G., Tannahill,D. and Balasubramanian,S. (2018) Genome-wide mapping of endogenous G-quadruplex DNA structures by chromatin immunoprecipitation and high-throughput sequencing. *Nat. Protoc.*, **13**, 551–564.
8. Balasubramanian,S., Hurley,L.H. and Neidle,S. (2011) Targeting G-quadruplexes in gene promoters: a novel anticancer strategy? *Nat. Rev. Drug Discov.*, **10**, 261–275.
9. Hänsel-Hertsch,R., Di Antonio,M. and Balasubramanian,S. (2017) DNA G-quadruplexes in the human genome: detection, functions and therapeutic potential. *Nat. Rev. Mol. Cell Biol.*, **18**, 279–284.
10. Biffi,G., Tannahill,D., Miller,J., Howat,W.J. and Balasubramanian,S. (2014) Elevated levels of G-quadruplex formation in human stomach and liver cancer tissues. *PLoS One*, **9**, e102711.
11. Platella,C., Riccardi,C., Montesarchio,D., Roviello,G.N. and Musumeci,D. (2017) G-quadruplex-based aptamers against protein targets in therapy and diagnostics. *Biochim. Biophys. Acta - Gen. Subj.*, **1861**, 1429–1447.
12. Musumeci,D., Platella,C., Riccardi,C., Merlino,A., Marzo,T., Massai,L., Messori,L. and Montesarchio,D. (2016) A first-in-class and a fished out anticancer platinum compound: *cis*-$[PtCl_2(NH_3)_2]$ and *cis*-$[PtI_2(NH_3)_2]$ compared for their reactivity towards DNA model systems. *Dalt. Trans.*, **45**, 8587–8600.
13. Musumeci,D., Platella,C., Riccardi,C., Moccia,F. and Montesarchio,D. (2017) Fluorescence sensing using DNA Aptamers in cancer research and clinical diagnostics. *Cancers (Basel)*, **9**, 174.
14. Platella,C., Guida,S., Bonmassar,L., Aquino,A., Bonmassar,E., Ravagnan,G., Montesarchio,D., Roviello,G.N., Musumeci,D. and Fuggetta,M.P. (2017) Antitumour activity of resveratrol on human melanoma cells: a possible mechanism related to its interaction with malignant cell telomerase. *Biochim. Biophys. Acta - Gen. Subj.*, **1861**, 2843–2851.
15. Platella,C., Raucci,U., Rega,N., D'Atri,S., Levati,L., Roviello,G.N., Fuggetta,M.P., Musumeci,D. and Montesarchio,D. (2020) Shedding light on the interaction of polydatin and resveratrol with G-quadruplex and duplex DNA: a biophysical, computational and biological approach. *Int. J. Biol. Macromol.*, **151**, 1163–1172.
16. Amato,J., Platella,C., Iachettini,S., Zizza,P., Musumeci,D., Cosconati,S., Pagano,A., Novellino,E., Biroccio,A., Randazzo,A. *et al.* (2019) Tailoring a lead-like compound targeting multiple G-quadruplex structures. *Eur. J. Med. Chem.*, **163**, 295–306.
17. Platella,C., Musumeci,D., Amato,J., Randazzo,A., Pagano,B. and Montesarchio,D. (2018) Method for the preparation of a low unspecific binding-support for affinity chromatography and/or on-line synthesis of oligonucleotides. EP3378556A1.
18. Platella,C., Musumeci,D., Arciello,A., Doria,F., Freccero,M., Randazzo,A., Amato,J., Pagano,B. and Montesarchio,D. (2018) Controlled Pore Glass-based oligonucleotide affinity support: towards high throughput screening methods for the identification of conformation-selective G-quadruplex ligands. *Anal. Chim. Acta*, **1030**, 133–141.
19. Musumeci,D., Amato,J., Zizza,P., Platella,C., Cosconati,S., Cingolani,C., Biroccio,A., Novellino,E., Randazzo,A., Giancola,C. *et al.* (2017) Tandem application of ligand-based virtual screening and G4-OAS assay to identify novel G-quadruplex-targeting chemotypes. *Biochim. Biophys. Acta - Gen. Subj.*, **1861**, 1341–1352.
20. Musumeci,D., Amato,J., Randazzo,A., Novellino,E., Giancola,C., Montesarchio,D. and Pagano,B. (2014) G-quadruplex on oligo affinity support (G4-OAS): an easy affinity chromatography-based assay for the screening of G-quadruplex ligands. *Anal. Chem.*, **86**, 4126–4130.
21. Platella,C., Pirota,V., Musumeci,D., Rizzi,F., Iachettini,S., Zizza,P., Biroccio,A., Freccero,M., Montesarchio,D. and Doria,F. (2020) Trifunctionalized naphthalene diimides and dimeric analogues as G-quadruplex-targeting anticancer agents selected by affinity chromatography. *Int. J. Mol. Sci.*, **21**, 1964.
22. Zuffo,M., Doria,F., Botti,S., Bergamaschi,G. and Freccero,M. (2017) G-quadruplex fluorescence sensing by core-extended naphthalene diimides. *Biochim. Biophys. Acta - Gen. Subj.*, **1861**, 1303–1311.
23. Salvati,E., Doria,F., Manoli,F., D'Angelo,C., Biroccio,A., Freccero,M. and Manet,I. (2016) A bimodal fluorescent and photocytotoxic naphthalene diimide for theranostic applications. *Org. Biomol. Chem.*, **14**, 7238–7249.
24. Doria,F., Manet,I., Grande,V., Monti,S. and Freccero,M. (2013) Water-soluble naphthalene diimides as singlet oxygen sensitizers. *J. Org. Chem.*, **78**, 8065–8073.
25. Collie,G.W., Promontorio,R., Hampel,S.M., Micco,M., Neidle,S. and Parkinson,G.N. (2012) Structural basis for telomeric G-quadruplex

targeting by naphthalene diimide ligands. *J. Am. Chem. Soc.*, **134**, 2723–2731.
26. Pirota,V., Nadai,M., Doria,F. and Richter,S.N. (2019) Naphthalene diimides as multimodal G-quadruplex-selective ligands. *Molecules*, **24**, 426.
27. Gunaratnam,M., de la Fuente,M., Hampel,S.M., Todd,A.K., Reszka,A.P., Schätzlein,A. and Neidle,S. (2011) Targeting pancreatic cancer with a G-quadruplex ligand. *Bioorganic Med. Chem.*, **19**, 7151–7157.
28. Ohnmacht,S.A., Marchetti,C., Gunaratnam,M., Besser,R.J., Haider,S.M., Di Vita,G., Lowe,H.L., Mellinas-Gomez,M., Diocou,S., Robson,M. *et al.* (2015) A G-quadruplex-binding compound showing anti-tumour activity in an in vivo model for pancreatic cancer. *Sci. Rep.*, **5**, 11385.
29. Neidle,S., Ohnmacht,S.A., Gunaratnam,M., Dale,A.G., Micco,M. and Collie,G.W. (2016) Diimide compounds. *US9*, **493**, 460B2.
30. Lopergolo,A., Perrone,R., Tortoreto,M., Doria,F., Beretta,G.L., Zuco,V., Freccero,M., Borrello,M.G., Lanzi,C., Richter,S.N. *et al.* (2016) Targeting of RET oncogene by naphthalene diimide-mediated gene promoter G-quadruplex stabilization exerts anti-tumor activity in oncogene-addicted human medullary thyroid cancer. *Oncotarget*, **7**, 49649–49663.
31. Neidle,S., Marchetti,C. and Ohnmacht,S.A. (2017) Substituted naphthalene diimides and their use. WO2017/103587A1.
32. Marchetti,C., Zyner,K.G., Ohnmacht,S.A., Robson,M., Haider,S.M., Morton,J.P., Marsico,G., Vo,T., Laughlin-Toth,S., Ahmed,A.A. *et al.* (2018) Targeting multiple effector pathways in pancreatic ductal adenocarcinoma with a G-quadruplex-Binding small molecule. *J. Med. Chem.*, **61**, 2500–2517.
33. Morales Sanchez,J.C., Perez-Victoria Moreno De Barreda,J.M., Arevalo Ruiz,M., Belmonte Reche,E., Martinez Garcia,M., Lucas Rodriguez,R., Freccero,M., Doria,F., Carda Usò,P.M., Falomir Ventura,E. *et al.* (2018) Naphthalene diimide compound for treatment of diseases. WO2018/060423A1.
34. Trajkovski,M., Endoh,T., Tateishi-Karimata,H., Ohyama,T., Tanaka,S., Plavec,J. and Sugimoto,N. (2018) Pursuing origins of (poly)ethylene glycol-induced G-quadruplex structural modulations. *Nucleic Acids Res.*, **46**, 4301–4315.
35. Luu,K.N., Tu,A., Kuryavyi,V., Lacroix,L. and Patel,D.J. (2006) Structure of the human telomere in K^+ solution: an intramolecular (3 + 1) G-quadruplex scaffold. *J. Am. Chem. Soc.*, **128**, 9963–9970.
36. Adrian,M., Heddi,B. and Phan,A.T. (2012) NMR spectroscopy of G-quadruplexes. *Methods*, **57**, 11–24.
37. Webba da Silva,M. (2007) NMR methods for studying quadruplex nucleic acids. *Methods*, **43**, 264–277.
38. Cavaluzzi,M.J. (2004) Revised UV extinction coefficients for nucleoside-5′-monophosphates and unpaired DNA and RNA. *Nucleic Acids Res.*, **32**, e13.
39. Atkins,P. and De Paula,J. (2006) In: *Physical Chemistry*. 8th edn, Oxford UP, Oxford.
40. Lapham,J., Rife,J.P., Moore,P.B. and Crothers,D.M. (1997) Measurement of diffusion constants for nucleic acids by NMR. *J. Biomol. NMR*, **10**, 255–262.
41. Giancola,C. and Pagano,B. (2013) Energetics of ligand binding to G-quadruplexes. *Top Curr. Chem.*, **330**, 211–242.
42. Huang,Y., Zhang,X., Ma,Z., Li,W., Zhou,Y., Zhou,J., Zheng,W. and Sun,C.Q. (2013) Size, separation, structural order, and mass density of molecules packing in water and ice. *Sci. Rep.*, **3**, 3005.
43. Fernandes,M.X., Ortega,A., Lopez Martinez,M.C. and Garcia de la Torre,J. (2002) Calculation of hydrodynamic properties of small nucleic acids from their atomic structure. *Nucleic Acids Res.*, **30**, 1782–1788.
44. Trajkovski,M. and Plavec,J. (2020) Chasing particularities of guanine- and cytosine-rich DNA strands. *Molecules*, **25**, 434.
45. Schnarr,L., Jana,J., Preckwinkel,P. and Weisz,K. (2020) Impact of a snap-back loop on stability and ligand binding to a parallel G-Quadruplex. *J. Phys. Chem. B*, **124**, 2778–2787.
46. Buchholz,I., Karg,B., Dickerhoff,J., Sievers-Engler,A., Lämmerhofer,M. and Weisz,K. (2017) Selective targeting of G-Quadruplex structures by a Benzothiazole-Based binding motif. *Chem. Eur. J.*, **23**, 5814–5823.
47. Funke,A., Dickerhoff,J. and Weisz,K. (2016) Towards the development of structure-selective G-quadruplex-binding indolo[3, 2-b]quinolines. *Chem. Eur. J.*, **22**, 3170–3181.
48. Brynn Hibbert,D. and Thordarson,P. (2016) The death of the Job plot, transparency, open science and online tools, uncertainty estimation methods and other developments in supramolecular chemistry data analysis. *Chem. Commun.*, **52**, 12792–12805.
49. Ulatowski,F., Dabrowa,K., Bałakier,T. and Jurczak,J. (2016) Recognizing the limited applicability of job plots in studying host-guest interactions in supramolecular chemistry. *J. Org. Chem.*, **81**, 1746–1756.
50. Sabharwal,N.C., Chen,J., Lee,J.H.J., Gangemi,C.M.A., D'urso,A. and Yatsunyk,L.A. (2018) Interactions between spermine-derivatized tentacle porphyrins and the human telomeric DNA G-quadruplex. *Int. J. Mol. Sci.*, **19**, 3686.
51. Hu,M.H., Chen,S.Bin, Wang,B., Ou,T.M., Gu,L.Q., Tan,J.H. and Huang,Z.S. (2017) Specific targeting of telomeric multimeric G-quadruplexes by a new triaryl-substituted imidazole. *Nucleic Acids Res.*, **45**, 1606–1618.
52. Guan,A.-J., Shen,M.-J., Xiang,J.-F., Zhang,E.-X., Li,Q., Sun,H.-X., Wang, Li,X., Xu,G.-Z., Tang,Y.-L., Xu,L.-J. *et al.* (2015) G-quadruplex induced chirality of methylazacalix[6]pyridine via unprecedented binding stoichiometry: en route to multiplex controlled molecular switch. *Sci. Rep.*, **20**, 10479.
53. Micco,M., Collie,G.W., Dale,A.G., Ohnmacht,S.A., Pazitna,I., Gunaratnam,M., Reszka,A.P. and Neidle,S. (2013) Structure-based design and evaluation of naphthalene diimide G-quadruplex ligands as telomere targeting agents in pancreatic cancer cells. *J. Med. Chem.*, **56**, 2959–2974.
54. Parkinson,G.N., Cuenca,F. and Neidle,S. (2008) Topology conservation and loop flexibility in quadruplex-drug recognition: crystal structures of Inter- and intramolecular telomeric DNA quadruplex-drug complexes. *J. Mol. Biol.*, **381**, 1145–1156.